



Ratiometric Sensing of Intracellular pH Based on Dual Emissive Carbon Dots

Yanli Sun¹ · Qin Wang¹ · Jin Liu¹ · Zuoping Zhao¹ · Lihua Li¹ · Zhifeng Liu¹ · Jiufu Lu¹ · Lingxia Jin¹ · Shengrui Zhang¹

Received: 16 September 2022 / Accepted: 28 November 2022 / Published online: 8 December 2022
© The Author(s), under exclusive licence to Springer Science+Business Media, LLC, part of Springer Nature 2022

Abstract

Accurate monitoring of intracellular pH in living cells is critical for developing a better understanding of cellular activities. In the current study, label-free carbon dots (*p*-CDs), which were fabricated using a straightforward one-pot solvothermal treatment of *p*-phenylenediamine and urea, were employed to create a new ratiometric pH nanosensor. Under single-wavelength excitation ($\lambda_{\text{ex}} = 500$ nm), the *p*-CDs gave dual emission bands at 525 and 623 nm. The fluorescent intensity ratio (I_{525}/I_{623}) was linearly related to pH over the range 4.0 to 8.8 in buffer solutions, indicating that the ratiometric fluorescence nanoprobe may be useful for pH sensing. In pH measurements, the *p*-CDs also demonstrated outstanding selectivity, reversibility, and photostability. Owing to the advantages outlined above, the nanoprobe was used to monitor the pH of HeLa cells effectively. The label-free CD-based ratiometric nanoprobe features comparatively easy manufacturing and longer excitation and emission wavelengths than the majority of previously reported CD-based ratiometric pH sensors, which is ultimately beneficial for applications in biological imaging.

Keywords Ratiometric nanosensor · Carbon dots · Label-free · Intracellular pH variation · Bioimaging

Introduction

Intracellular pH is a key target parameter in cell growth and death, muscle contraction, metabolism of organs, ion transport and homeostasis [1]. Abnormal intracellular pH values may cause various cardiopulmonary and neurological diseases, such as ischemic/reperfusion injury and Alzheimer's and Parkinson's disease [2]. Therefore, accurate intracellular pH monitoring is critical for developing a better understanding of cellular activities and providing crucial support in early disease identification. To date, the glass pH electrode is the most common tool used for pH measurement. However, the disadvantages of electrical interference or mechanical damage to cells cannot be avoided, making it unsuitable for intracellular pH studies [3]. In contrast, fluorescence-based

sensors are more applicable to detection of intracellular pH changes because they are noninvasive and exhibit excellent spatial and temporal resolution, good sensitivity and ease of sample preparation [4, 5]. However, the majority of fluorescent pH sensors are dependent on changes of a single emission intensity, which can be affected by a range of parameters, such as fluorescence probe concentration and dye bleaching, thereby reducing the reliability of the measured data [6]. Keeping this in mind, considerable effort has been devoted to developing ratiometric pH sensors that can self-calibrate to overcome interference by environmental factors and successfully exceed the limits of single emission intensity measurements.

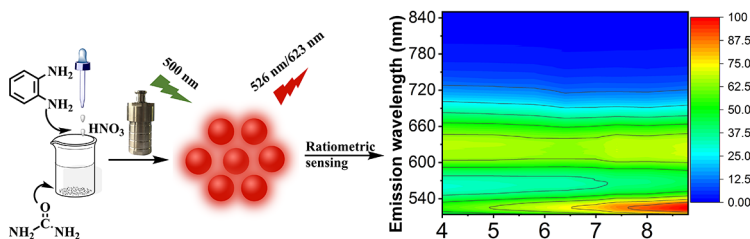
Carbon dots (CDs) have recently attracted much interest due to their small particle sizes, nonblinking properties, low toxicity, excellent solubility and biocompatibility [7–11]. In recent years, several groups have created many ratiometric fluorescent pH sensors based on CDs and used them to monitor intracellular pH [12–18]. Ma et al., for example, combined pH-insensitive rhodamine B isothiocyanate, pH-sensitive fluorescein isothiocyanate, and amino-coated CDs into a single device to create a programmable ratiometric pH sensor [19]. Using CD-fluorescein isothiocyanate composites, Wang et al. fabricated a fluorescent ratiometric pH

✉ Qin Wang
qincaimuxu009@sina.cn

✉ Shengrui Zhang
zhangshr09@sina.com

¹ Shaanxi Key Laboratory of Catalysis, School of Chemistry and Environment Science, Shaanxi University of Technology, 723000 Hanzhong, Shaanxi, China

Scheme 1 Schematic illustration of *p*-CD preparation and application for ratiometric determination of pH



probe [20]. However, these ratiometric pH-sensing devices involved cross-attachment or embedding of dyes in the CDs, and extensive separation and purification operations were still required [21]. To circumvent the disadvantages highlighted above, numerous ratiometric fluorescence nanosensors based on label-free CDs have been developed [22, 23]. For example, Yang et al. synthesized novel ratiometric fluorescent CDs for enantioselective sensing of L-lysine and pH in vivo and in vitro [24]. A novel ratiometric fluorescence nanosensor incorporating label-free CDs was constructed by Feng et al. for intracellular water pH monitoring and lysosome imaging [25]. Nevertheless, the development of CD-based fluorescent probes appropriate for measuring pHs in living cells is at an initial level [26, 27]. As a result, it is critical to construct CDs with pH-sensitive ratiometric fluorescence emission to develop ratiometric fluorescence nanoprobes for pH assessments in living cells.

A ratiometric fluorescent pH nanoprobe comprising label-free CDs was constructed in this work and utilized for intracellular pH sensing, as shown in Scheme 1. The preparation of CDs (*p*-CDs) exhibiting dual emission at 525 and 623 nm was achieved with a one-pot solvothermal treatment of *p*-phenylenediamine (*p*-PD) and urea. The *p*-CDs showed inherent ratiometric fluorescence emission (I_{525}/I_{623}) as a function of pH change without the necessity for dye labeling, and exhibited a strong linear relationship with pH over the response range 4.0–8.8 in buffer solutions. The CDs, owing to their unique emission features, were subsequently used as a ratiometric fluorescent pH nanoprobe to monitor the pHs of HeLa cells.

Experimental Section

Materials

p-PD, urea, glutathione (GSH), cysteine (Cys), homocysteine (Hcy), alanine (Ala), arginine (Arg), serine (Ser), leucine (Leu), and metal ions were procured from Aladdin Ltd. (<http://www.aladdin-e.com/>, Shanghai, China). The rest of the chemicals were of analytical grade, and no additional purification was carried out before utilization in experiments. Throughout the research, distilled water was used.

Characterization

TEM micrographs were obtained using a GZF2.0 FEI Electron Optics transmission electron microscope (Thermo Scientific, America <https://www.thermofisher.com/>). An ESCALAB 250Xi multitechnique surface analyzer was used to perform X-ray photoelectron spectroscopy (XPS) studies (Thermo Scientific, America <https://www.thermofisher.com/>). KBr pellets were used to acquire Fourier transform infrared (FT-IR) spectra on a Tensor 27 FT-IR spectrometer (Bruker, Germany <https://www.bruker.com/>). A Shimadzu UV-2550 spectrophotometer was used to record absorption values (Shimadzu, Japan <https://www.shimadzu.com>). An RF5301 fluorescence spectrometer was used to measure all fluorescence spectra (Shimadzu, Japan <https://www.shimadzu.com>). The fluorescent lifetimes and absolute quantum yields were determined with an Edinburgh Analytical FLS1000 instrument (Techcomp, China) (Techcomp, China <http://www.techcomp.cn/>). A Sartorius PB-10 pH meter was used to measure pH (Sartorius, Germany <https://www.sartorius.com.cn/>). A Xiangyi H1650-W centrifuge was used to separate mixtures (Xiangyi, China <http://www.xiangyi-hn.com/>). A Carl Zeiss LSM 880 confocal laser scanning microscope was used for fluorescence imaging (Zeiss, Germany <https://www.zeiss.com/corporate/int/home.html>).

Preparation of CDs

The *p*-CDs were prepared through a one-pot solvothermal method according to literature reports [28, 29]. Carbonization of *p*-PD and urea with the help of concentrated HNO₃ was used to generate *p*-CDs via a solvothermal technique. First, 0.1 g of *p*-PD and 0.1 g of urea were dissolved in C₂H₅OH (10 mL). Subsequently, the solution was poured into a 25 mL poly(tetrafluoroethylene)-lined stainless steel autoclave. Afterward, 40 μL of pure HNO₃ was added dropwise with vigorous stirring. A dark-red suspension was formed after heating for 12 h at 180 °C, and the solution was left to cool to room temperature. To eliminate the nonfluorescent precipitates, the solution was subjected to centrifugation for 15 min at 12,000 rpm (with a 10,000×g centrifugation force). The products were purified on a silica column using methanol and methylene dichloride as the eluent, and the *p*-CDs were separated for use as nanosensors.

The CD sample was eventually obtained following evaporation of the solvent and drying in a vacuum, and the absolute quantum yield of *p*-CDs emission was 8%.

Fluorescence Assays of pH Values

To make a stock solution, the *p*-CDs were dissolved in ethanol. pH values were determined using a 20 mM buffer containing disodium hydrogen phosphate-citric acid buffer at pHs 2.2–8.0 and a glycine-sodium hydroxide buffer at pHs 8.5–10.6. A 100 μ L CD dispersion (1.0 mg/mL) was added to 4.90 mL of buffer at various pH levels in a series of test tubes. The resultant solutions were mixed well before fluorescence spectra were taken. By altering the pH values between 5.0 and 8.0 with HCl and NaOH solutions, the reversibility of CD suspension was studied after repetition for four continual cycles, and the fluorescence spectra were obtained. The tests were carried out in triplicate.

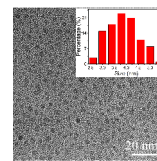
Cytotoxicity Assay

A conventional 3-(4,5-dimethyl-2-thiazolyl)-2,5-diphenyl-2 H-tetrazolium bromide (MTT) test was employed to examine the cytotoxicity of the *p*-CDs. Ninety-six-well plates were used to seed HeLa cells for 24 h prior to treatment, and they were subsequently cultured for 12 h with various doses of *p*-CDs (0–60 μ g/mL). Next, 20 μ L of MTT solution (5.0 mg/mL) was added to the individual wells and incubated for 4 h at 37 °C. Then, 100 μ L of supernatant was withdrawn, and 150 μ L of dimethyl sulfoxide (DMSO) was added to the individual wells for solubilization of formazan. The plate was agitated for 10 min before a microplate reader was employed for absorbance measurements of the solutions at 562 nm. All MTT tests were carried out four times in total.

Cell Fluorescence Imaging

HeLa cells were seeded on 6-well culture plates with sterile coverslips and left to adhere for 24 h before investigation. The media was withdrawn, and the cells were subjected to treatment for 5 h at 37 °C with *p*-CDs (40 μ g/mL) in RPMI medium. Phosphate buffered saline (PBS) (pH 7.4) was then utilized to wash the cells three times. It was subsequently incubated for 30 min with 5 μ g/mL nigericin in a high concentration K^+ buffer at various pH values (5.0, 7.0, and 8.0). A Carl Zeiss LSM 880 confocal laser scanning microscope was used to image the cells immediately. The excitation wavelength was 458 nm, while the emission collection wavelength range was 475–575 nm.

Fig. 1 TEM image and histogram showing the particle size distribution (inset) of the *p*-CDs.



Results and Discussion

Characterization of *p*-CDs

TEM was first employed to assess the morphological features of the *p*-CDs. The *p*-CDs were spherical and exhibited good dispersion in aqueous solutions, as shown in Fig. 1. Furthermore, their size distribution was determined to be 2.6–5.4 nm, with a mean size of 3.8 nm (based on measurements of more than 100 particles in the TEM photograph) (inset of Fig. 1).

The surface functional groups and elemental compositions were then determined using XPS analysis and FT-IR spectroscopy. According to the survey spectrum, the main components of the targeted CDs were carbon, oxygen, and nitrogen: 78.48% carbon, 7.69% oxygen, and 13.83% nitrogen (Fig. 2 A). The high-resolution C 1s XPS spectrum (Fig. 2B) was deconvoluted into three peaks at 284.78, 287.13, and 290.43 eV that were ascribed to C-C/C=C, C-N/C=O, and O-C=O bonds, respectively [24, 30]. The high-resolution N 1s spectrum (Fig. 2 C) showed a pair of peaks at 399.48 and 402.08 eV, corresponding to pyridinic and amino N bonds, respectively [31, 32]. Oxygens on carbon atoms (C=O/C-OH) (Fig. 2D) were identified in the high resolution O 1s spectrum with a peak at 531.63 eV [33]. FT-IR characterization was also carried out for analysis of chemical bonding on the surfaces of the *p*-CDs. The FT-IR spectrum of the *p*-CDs is shown in Fig. 3 A, which demonstrates that the *p*-CDs contained $-NH_2$ (3301 and 3203 cm^{-1}), $-CH_2$ (3008 cm^{-1}), O=C-O- (1759 cm^{-1}), C=C (1630 cm^{-1}), $-C=N$ (1517 cm^{-1}), C-N-C (1261 cm^{-1}), and C-O-C (1128 cm^{-1}) functional groups [34–36]. The results of the FT-IR and XPS analyses were similar, indicating that $-NH_2$ and $-COOH$ groups existed on the *p*-CD surface, rendering it highly water-soluble. The chemically reactive entities also allowed further functionalization and surface passivation.

Optical Features of the *p*-CDs

The optical features of the *p*-CDs were examined by collecting their absorption and fluorescence spectra. The *p*-CDs in aqueous solutions exhibited numerous absorption bands at 241, 296, and 400–550 nm, as shown in Fig. 3B. The aromatic C=C bonds gave rise to $n-\pi^*$ transitions, which were responsible for the absorption bands at 241 and 296 nm

Fig. 2 Structural characterization of the *p*-CDs. (A) XPS survey spectrum; high-resolution XPS survey scans for (B) C 1s, (C) N 1s and (D) O 1s binding energies of the *p*-CDs.

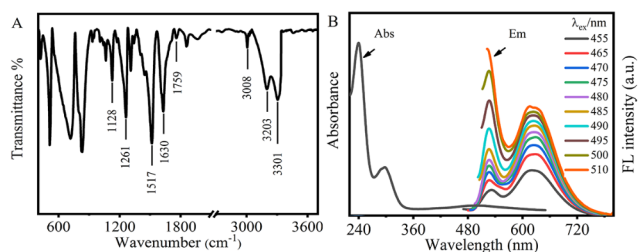
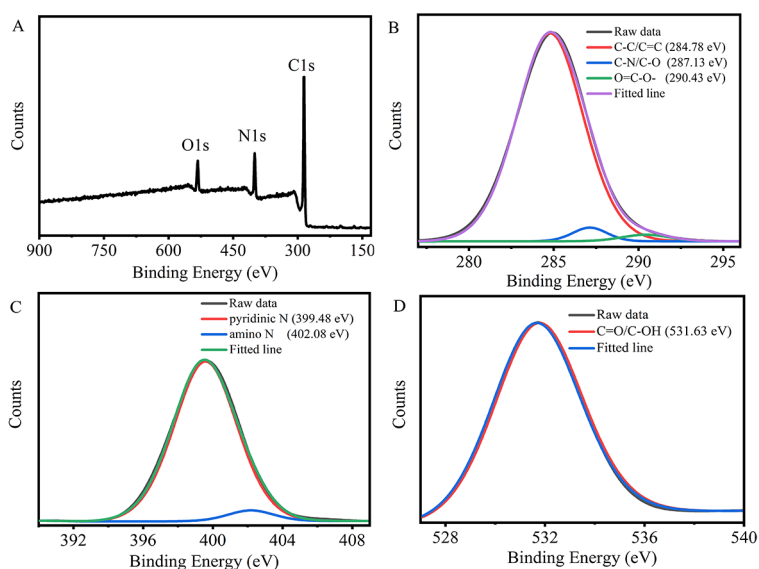


Fig. 3 (A) FT-IR spectrum of *p*-CDs; (B) Absorption (Abs) and fluorescence emission spectra (Em) of *p*-CDs with various excitation wavelengths

[37], and the wide absorption between 400 and 550 nm was ascribed to $n-\pi^*$ transitions occurring with the surface states of *p*-CDs [38, 39]. Next, the fluorescence characteristics of the *p*-CDs were thoroughly investigated. The fluorescence intensities of the *p*-CDs at 525 and 623 nm increased with increasing excitation wavelength, as shown in Fig. 3B. However, the emission spectrum at 525 nm was not fully displayed when the wavelength excitation was 510 nm.

Therefore, an excitation wavelength of 500 nm was selected as the excitation maximum in this study, which was facilitated by ratiometric detection of pH. Furthermore, when the excitation wavelength was varied from 325 to 405 nm, the emission wavelengths of the *p*-CDs remained nearly unchanged. This excitation independence may be attributed to the remarkable chemical composition and content uniformity of the *p*-CDs [40], which may enable expanded biological applications by avoiding autofluorescence [41].

Investigation of pH-Response Properties

Using 20 mM buffer with various pH values in the range 4.0 to 8.8, standard fluorescence pH titrations of the *p*-CDs were carried out. As shown by the 3D emission-pH spectra (Fig. 4 A), the fluorescence emission intensity at 525 nm underwent a progressive increase with increasing pH values, whereas the emission intensity at 623 nm for the *p*-CDs remained more or less constant. Fluorescence

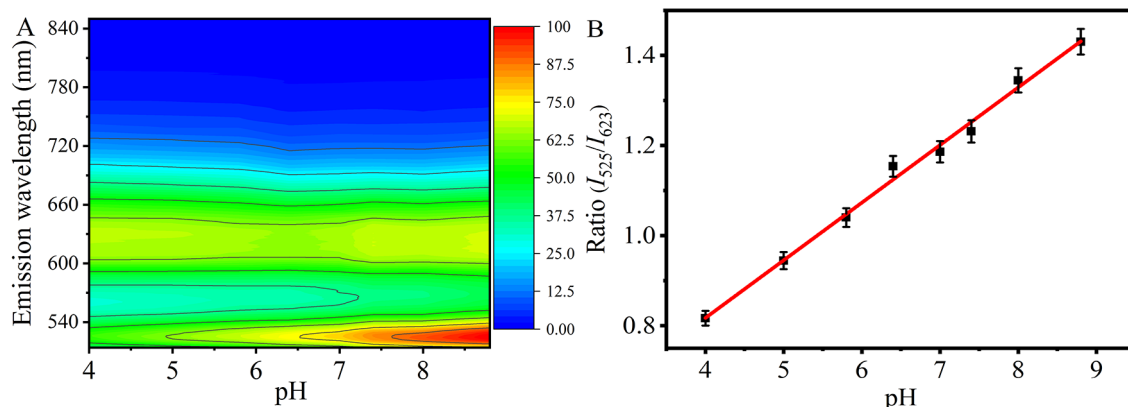


Fig. 4 (A) 3D emission-pH spectra of *p*-CDs in 20 mmol/L buffer at different pH values; (B) Linear relationship of the fluorescence intensity ratio ($I_{525\text{ nm}}/I_{623\text{ nm}}$) versus pH. $\lambda_{\text{ex}} = 500\text{ nm}$

Fig. 5 (A) UV–vis absorption spectra of the as-prepared *p*-CDs in different pH buffers; (B) Normalized transient intensity of *p*-CDs on the nanosecond timescale

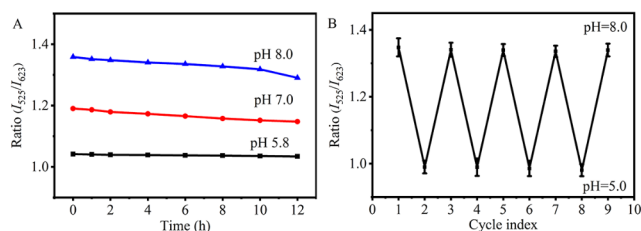
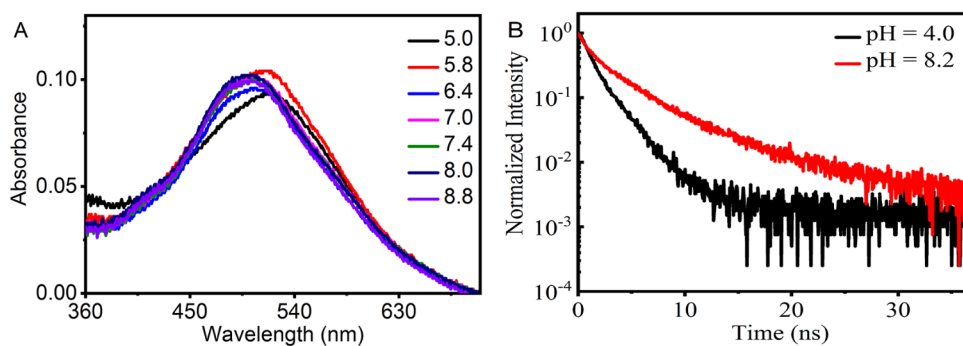


Fig. 6 (A) Time-dependent fluorescence intensity changes of *p*-CDs in buffer solutions with different pH values in daylight for 12 h; (B) Fluorescence reversibility versus pH for repeated changes of pH between 5.0 and 8.0

emission spectra also confirmed this result (Fig. S1). The intensity ratios of the two emission channels (I_{525}/I_{623}) manifested a linear relationship with pH over the range 4.0 to 8.8 and were fit with the linear regression equation $I_{525}/I_{623} = 0.1279\text{pH} + 0.3057$, with a linear coefficient of 0.9968 (Fig. 4B). The linear range was wide enough to suit the needs of intracellular pH monitoring and in vivo imaging. The aforementioned findings showed that *p*-CDs might be used as a novel nanoprobe for quantitatively determining pH levels.

We initially looked at the UV–vis spectra of *p*-CDs as the pH was increased from 4.0 to 8.8 to see if we could determine the cause of the response to pH. There was no discernible change, as indicated in Fig. 5 A. As a result, we concluded that the increased fluorescence of the *p*-CDs at high pH levels could not be due to aggregation [42]. Then, fluorescence lifetime measurements were measured (Fig. 5B). The fluorescence decays of the *p*-CD solutions remained biexponential as the pH was increased from 4.0 to 8.0, and the mean lifetimes rose from 1.70 to 4.31 ns, showing that the rate of nonradiative transitions was reduced. As a result, we hypothesized that the increased fluorescence intensity was due to the carboxylate-based negatively charged protective shell present on the surfaces of the *p*-CDs, which, in turn, restricted the rate of nonradiative decay from the photoexcited state of the *p*-CDs and resulted in a significant improvement in fluorescence [43].

Photostability and Reversibility of *p*-CDs

Since excellent photostability and reversibility are essential for long-term and real-time cellular imaging, we further investigated the photostability and reversibility of the *p*-CDs. Timed scans for measurements of fluorescence intensity in 20 mM PBS buffer with varying pH values (5.8, 7.0, and 8.0) were conducted for 12 h to examine the photostability. The ratiometric fluorescence intensities (I_{525}/I_{623}) of the *p*-CDs remained uniform during the scanning process (Fig. 6 A), which performed that they were stable to air and light at appropriate pH values. The fluorescence reversibility as a function pH was then tested by repeatedly altering the pH between 5.0 and 8.0. The ratiometric fluorescence intensity (I_{525}/I_{623}) of the carbon dots showed high consistency for the alkaline (pH 8.0) and acidic (pH 5.0) solutions, as shown in Fig. 6B. Thus, the pH-sensitive CDs demonstrated satisfactory fluorescence reversibility and photostability in solutions with a range of pH values, indicating that they might be utilized as intracellular pH nanoprobe.

Influence of Potentially Interfering Substances in Solutions with Varying pH Values

The possible interference resulting from high quantities of amino acids (Ala, Arg, Ser, and Leu), biothiols (GSH, Cys, and Hcy), and metallic ions (Ca^{2+} , Mg^{2+} , Al^{3+} , Zn^{2+} , Cu^{2+} , Ni^{2+} , Mn^{2+} , Pb^{2+} , Hg^{2+} , Fe^{2+} , Fe^{3+} , Cd^{2+} , and Ag^{+}) was explored. As demonstrated in Fig. 7, there were no substantial variations in the fluorescence intensities of the *p*-CDs in the presence of these interfering chemicals, indicating remarkable selectivity for the nanoprobe.

pH Imaging in Living Cells

The use of *p*-CDs for determining the pH values of HeLa cells was attempted after the abovementioned results were obtained. To assess the toxicity of *p*-CDs to live cells, a conventional MTT test was first used [44]. As demonstrated in Fig. S2, there was no substantial reduction in cell viability, demonstrating that *p*-CDs had limited cytotoxicity toward

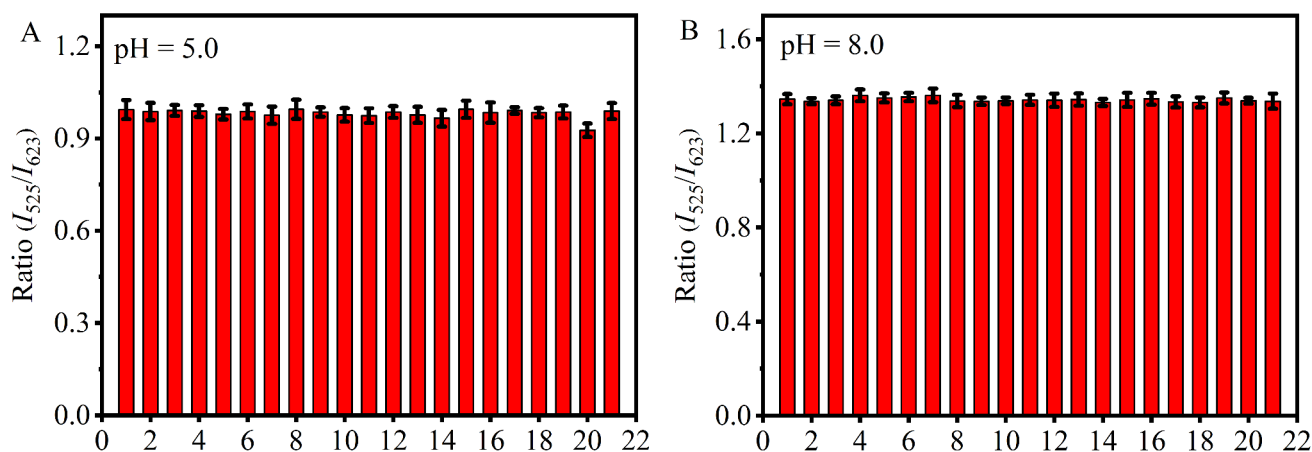


Fig. 7 Fluorescence intensity of *p*-CDs in the presence of interfering substances in 20 mM PBS buffer with different pH values. 1, Blank; 2, Ca^{2+} ; 3, Mg^{2+} ; 4, Al^{3+} ; 5, Zn^{2+} ; 6, Cu^{2+} ; 7, Ni^{2+} ; 8, Mn^{2+} ; 9, Pb^{2+} ; 10,

Hg^{2+} ; 11, Fe^{2+} ; 12, Fe^{3+} ; 13, Cd^{2+} ; 14, Ag^{+} ; 15, Ala; 16, Arg; 17, Ser; 18, Leu; each concentration was 1 mM. 19, 5 mM GSH; 20, 0.5 mM Hcy; 21, 0.5 mM Cys. (A) pH at 5.0, (B) pH at 8.0

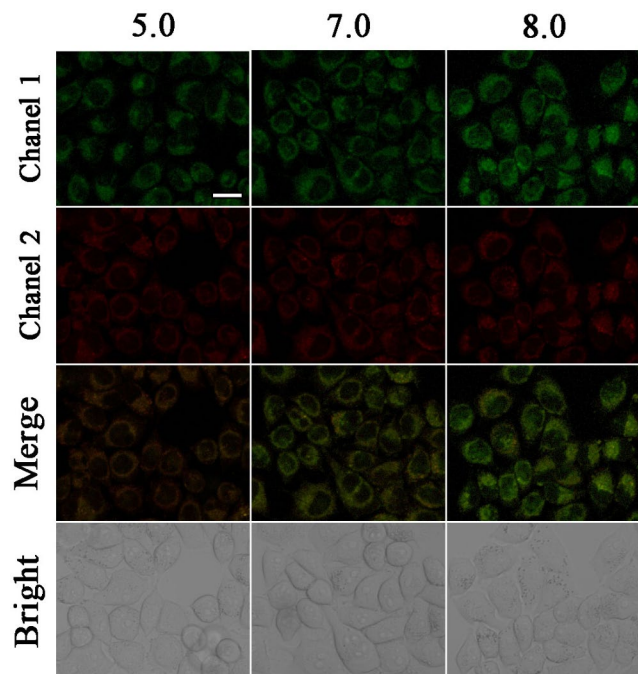


Fig. 8 Confocal microscope fluorescence images of 40 µg/mL *p*-CDs incubated with HeLa cells in high concentration K^{+} buffer at different pH values. Excitation wavelength for *p*-CDs: 458 nm; emission collection: 475–575 nm. Scale bar: 20 µm

HeLa cells at concentrations below 60 µg/mL. HeLa cells were then treated with *p*-CDs (40 µg/mL) for 5 h at 37 °C to look for subtle alterations in the intracellular pH. The cells were then treated for 30 min with buffers establishing pH values of 5.0, 7.0, and 8.0, which allowed for $\text{H}^{+}/\text{K}^{+}$ exchange and maintained an equal pH in the buffer media and inside the cells [45, 46]. As depicted in Fig. 8, the emission intensity of the treated cells in channel 1 (green pseudocolor) increased progressively as the pH was raised from

5.0 to 8.0, but channel 2 (red pseudocolor) remained nearly unaltered. The merged graphs of channel 1 and channel 2 exhibited a noticeable hue shift with pH changes. In addition, Picture-Pro Plus software was used to create a fluorescence ratio image ($I_{\text{green}}/I_{\text{red}}$) (Fig. S3). The intensity ratio (I_{525}/I_{623}) was linearly related to pH over range 5.0–8.0, as predicted, demonstrating that the CD-based nanoprobe is capable of detecting subtle changes in intracellular pH.

Finally, comparisons between this ratiometric nanosensor and other published CD-based ratiometric sensors used for pH detection in materials, including their diameters, excitation and emission wavelengths, and measurement ranges, are summarized in Table 1 [16, 23, 25, 47–53]. This nanosensor presented longer excitation and emission wavelengths ($\lambda_{\text{ex}} = 500$ nm; $\lambda_{\text{em}} = 526/623$ nm), a wider linear range (4.0–8.8) and simpler synthetic procedures (one-pot solvothermal method) than the other CD-based pH sensors, making this nanosensor comparable to previous CD-based ratiometric sensors. The relatively small Stokes shift is the major limitation of the *p*-CDs, and this can be modified by constructing CDs with larger Stokes shifts to extend the scope of applications involving sensitive measurements of intracellular pH.

Conclusion

A simple one-pot solvothermal carbonization process was used to generate novel nanoprobe *p*-CDs. Detailed spectroscopic characterization revealed that this novel fluorescent nanoprobe may be utilized to monitor pH in ratiometrically by using emission intensities at the two wavelengths 525 and 623 nm. The fluorescence intensity ratios (I_{525}/I_{623}) for *p*-CDs increased with increasing pH from 4.0 to 8.8 and

Table 1 A comparison of CD-based methods for detection of pH value

Materials	Method	Diameter (nm)	E_x/E_m (nm)	Measurement Range (pH values)	Limitations	Ref.
Label-free CDs	Ratiometric fluorescence imaging	2.47	380/440, 542	2.0–3.4; 3.4–8.0	Short wavelength excitation	[16]
Label-free CDs	Ratiometric fluorescence imaging	3.5	310/336, 540	2.5–12.0	Short wavelength excitation	[23]
Label-free CDs	Ratiometric fluorescence imaging	6.2	365/415, 555	4.5–6.5	Short wavelength excitation	[25]
Label-free CDs	Ratiometric fluorescence imaging	2.0	350/410, 565	4.5–6.5; 10.0–13.0	Short wavelength excitation; Not suitable for neutral system	[47]
Ag ₂ S CDs nanohybrids	Ratiometric fluorescence imaging	4.7 ± 0.4	450/500, 670	5.4–6.8	Relatively complex synthesis procedures; Narrow linear range	[48]
Rhodamine B/CDs	Ratiometric fluorescence imaging	2.3 ± 0.38	400/467, 580	4.0–8.0	Relatively complex synthesis procedures	[49]
Rhodamine B/CDs	Ratiometric fluorescence imaging	5.7	325/400, 582	8.3–11.2	Short wavelength excitation	[50]
CDs/CdTe quantum dots	Ratiometric fluorescence imaging	3.6	330/430, 600	3.0–11.0	Relatively complex synthesis procedures; Short wavelength excitation	[51]
Label-free CDs	Ratiometric fluorescence imaging	1.4	290/365, 439	4.2–6.4	Short wavelength excitation and emission	[52]
Label-free CDs	Ratiometric fluorescence imaging	7.9	380/475, 545	5.2–8.8	Short wavelength excitation	[53]
Label-free CDs	Ratiometric fluorescence imaging	3.8	500/526, 623	4.0–8.8	Relatively small Stokes shift	This work

showed a linear relationship. This sensor could be used effectively to ratiometrically monitor pH changes in living cells due to its excellent selectivity, strong photostability, and fluorescence reversibility, suggesting practical applications for detection of pH-related diseases and disorders.

Supplementary Information The online version contains supplementary material available at <https://doi.org/10.1007/s10895-022-03107-w>.

Authorship Contribution Yanli Sun contributed to the methodology, investigations, probe preparation, data collection and curation, and writing-original draft preparation. Jin Liu, Zuoping Zhao, Lihua Li, and Zhifeng Liu contributed to methodology development, data collection, and sample pretreatment. Jiufu Lu and Lingxia Jin contributed to the formal analyses and validation. Qin Wang and Shengrui Zhang performed conceptualization, supervision, writing-reviewing and editing. All authors read and approved the final manuscript.

Funding The authors acknowledge financial support from the National Natural Science Foundation of China (Nos. 22177066), Innovation Capability Support Program of Shaanxi (No. 2021KJXX-51), Coconstruction Project of Hanzhong city and Shaanxi University of Technology (SXJ-2103, SXJ-2105) and Open Foundation of Key Laboratory of Synthetic and Natural Functional Molecule Chemistry of Ministry of Education (KLSNFM2020007).

Code Availability Not applicable.

Data Availability All data generated or analyzed of this study are available within the article.

Declarations

Ethics Approval Not applicable.

Consent to Participate Not applicable.

Consent for Publication Not applicable.

Conflict of Interest The authors declare that they have no competing.

References

- Ohkuma S, Poole B (1978) Fluorescence probe measurement of the intralysosomal pH in living cells and the perturbation of pH by various agents. *Proc Natl Acad Sci* 75(7):3327–3331. <https://doi.org/10.1073/pnas.75.7.3327>
- Kennedy RT, Huang L, Aspinwall CA (1996) Extracellular pH is required for rapid release of insulin from Zn-insulin precipitates in β -cell secretory vesicles during exocytosis. *J Am Chem Soc* 118(7):1795–1796. <https://doi.org/10.1021/ja953271w>
- Wan SL, Zheng Y, Shen J, Yang WT, Yin MZ (2014) “On-off-on” switchable sensor: a fluorescent spiropyran responds to extreme pH conditions and its bioimaging applications. *ACS Appl Mater Inter* 6(22):19515–19519. <https://doi.org/10.1021/am506641t>
- Chen Y (2021) Recent advances in fluorescent probes for extracellular pH detection and imaging. *Anal Biochem* 612:113900. <https://doi.org/10.1016/j.ab.2020.113900>
- Dangi V, Baral M, Kanungo BK (2020) Study on the development of a cyclohexane based tripodal molecular device as “off-on-off” pH sensor and fluorescent iron sensor. *Curr Anal Chem* 16(5):620–630. <https://doi.org/10.2174/1573411015666-190314154126>
- Liu LY, Zhao YP, Zhang N, Wang KN, Tian MG, Pan QL, Lin WY (2021) Ratiometric fluorescence imaging for the distribution of nucleic acid content in living cells and human tissue sections. *Anal Chem* 93(3):1612–1619. <https://doi.org/10.1021/acs.analchem.0c04064>
- Li S, Li L, Tu HY, Zhang H, Silvester DS, Banks CE, Zou GQ, Hou HS, Ji XB (2021) The development of carbon dots: from the perspective of materials chemistry. *Mater Today* 51:188–207. <https://doi.org/10.1016/j.mattod.2021.07.028>

8. Wareing TC, Gentile P, Phan AN (2021) Biomass-based carbon dots: current development and future perspectives. *ACS Nano* 15(10):15471–15501. <https://doi.org/10.1021/acsnano.1c03886>
9. Sk MP, Sailapu SK, Chattopadhyay A (2015) Luminescent carbon dots for logic operations in two phases. *ChemPhysChem* 16(4):723–727. <https://doi.org/10.1002/cphc.201402747>
10. Arshad F, Pal A, Alam T, Khan JA, Sk MP (2020) Luminescent carbogenic dots for the detection and determination of hemoglobin in real samples. *New J Chem* 44(16):6213–6221. <https://doi.org/10.1039/D0NJ00401D>
11. Arshad F, Sk MP (2019) Aggregation-induced red shift in N, S-doped chiral carbon dot emissions for moisture sensing. *New J Chem* 43(33):13240–13248. <https://doi.org/10.1039/C9NJ03009C>
12. Macairan JR, Zhang I, Clermont-Paquette A, Naccache R, Maysinger D (2020) Ratiometric pH sensing in living cells using carbon dots. *Part Part Syst Char* 37(1):2070002. <https://doi.org/10.1002/ppsc.202070002>
13. Du FK, Ming YH, Zeng F, Yu CM, Wu SZ (2013) A low cytotoxic and ratiometric fluorescent nanosensor based on carbon-dots for intracellular pH sensing and mapping. *Nanotechnology* 24(36):365101. <https://doi.org/10.1088/0957-4484/24/36/365101>
14. Hu SL, Meng X, Tian F, Yang WL, Li N, Xue CR, Yang JL, Chang Q (2017) Dual photoluminescence centers from inorganic-salt-functionalized carbon dots for ratiometric pH sensing. *J Mater Chem C* 5(38):9849–9853. <https://doi.org/10.1039/C7TC03266H>
15. Lesani P, Singh G, Lu Z, Mirkhalaf M, New EJ, Zreiqat H (2022) Two-photon ratiometric carbon dot-based probe for real-time intracellular pH monitoring in 3D environment. *Chem Eng J* 433(3):133668. <https://doi.org/10.1016/j.cej.2021.133668>
16. Long RQ, Tang C, Li T, Tong X, Tong CY, Guo Y, Gao QP, Wu LH, Shi SY (2020) Dual-emissive carbon dots for dual-channel ratiometric fluorometric determination of pH and mercury ion and intracellular imaging. *Microchim Acta* 187(5):307. <https://doi.org/10.1007/s00604-020-04287-7>
17. Pal A, Ahmad K, Dutta D, Chattopadhyay A (2019) Boron doped carbon dots with unusually high photoluminescence quantum yield for ratiometric intracellular pH sensing. *ChemPhysChem* 20(8):1018–1027. <https://doi.org/10.1002/cphc.201900140>
18. Wang X, Zhao L, Hu JS, Wei H, Liu XY, Li E, Yang SH (2022) Rational design of novel carbon-oxygen quantum dots for ratiometrically mapping pH and reactive oxygen species scavenging. *Carbon* 190:115–124. <https://doi.org/10.1016/j.carbon.2022.01.006>
19. Shi W, Li XH, Ma HM (2012) A tunable ratiometric pH sensor based on carbon nanodots for the quantitative measurement of the intracellular pH of whole cells. *Angew Chem Int Edit* 51(26):6432–6435. <https://doi.org/10.1002/anie.201202533>
20. Zhu XX, Jin H, Gao CL, Gui RJ, Wang ZH (2017) Ratiometric, visual, dual-signal fluorescent sensing and imaging of pH/copper ions in real samples based on carbon dots-fluorescein isothiocyanate composites. *Talanta* 162(1):65–71. <https://doi.org/10.1016/j.talanta.2016.10.015>
21. Xu SM, He X, Huang YB, Liu X, Zhao LH, Wang XH, Sun Y, Ma PY, Song DQ (2020) Lysosome-targeted ratiometric fluorescent sensor for monitoring pH in living cells based on one-pot-synthesized carbon dots. *Microchim Acta* 187:478. <https://doi.org/10.1007/s00604-020-04462-w>
22. Xia C, Cao MM, Xia JF, Zhou GH, Jiang DY, Zhang DF, Wang J, Li HL (2019) An ultrafast responsive and sensitive ratiometric fluorescent pH nanoprobe based on label-free dual-emission carbon dots. *J Mater Chem C* 7:2563–2569. <https://doi.org/10.1039/C8TC05693E>
23. Hamd-Ghadareh S, Salimi A, Fathi F, Soleimani F (2019) Dual-emission carbon dots as biocompatible nanocarrier for in vitro/in vivo cell microenvironment ratiometric pH sensing in broad range. *J Iran Chem Soc* 16(10):2081–2092. <https://doi.org/10.1007/s13738-019-01678-3>
24. Chang D, Zhao ZH, Shi H, Feng JY, Yang YX, Shi LH (2022) Ratiometric fluorescent carbon dots for enantioselective sensing of L-lysine and pH discrimination in vivo and in vitro. *Sens Actuata B-Chem* 362:131792. <https://doi.org/10.1016/j.snb.2022.131792>
25. Li SR, Song XR, Wang YH, Hu ZR, Yan F, Feng GD (2021) Developed a ratiometric fluorescence pH nanosensor based on label-free carbon dots for intracellular lysosome imaging and water pH monitoring with a smartphone. *Dyes Pigm* 193:109490. <https://doi.org/10.1016/j.dyepig.2021.109490>
26. He C, Xu P, Zhang XH, Long WJ (2022) The synthetic strategies, photoluminescence mechanisms and promising applications of carbon dots: current state and future perspective. *Carbon* 186:91–127. <https://doi.org/10.1016/j.carbon.2021.10.002>
27. Das P, Maruthapandi M, Saravanan A, Natan M, Jacobi G, Banin E, Gedanken A (2020) Carbon dots for heavy-metal sensing, pH-sensitive cargo delivery, and antibacterial applications. *ACS Appl Nano Mater* 3(12):11777–11790. <https://doi.org/10.1021/acsnanm.0c02305>
28. Lesani P, Lu Z, Singh G, Mursi M, Mirkhalaf M, New EJ, Zreiqat H (2021) Influence of carbon dot synthetic parameters on photophysical and biological properties. *Nanoscale* 13(25):11138–11149. <https://doi.org/10.1039/D1NR01389K>
29. Wang Q, Tang ZH, Li L, Guo JX, Jin LX, Lu JF, Huang P, Zhang SR, Jiao (2022) Highly efficient red-emitting carbon dots as a “turn-on” temperature probe in living cells. *Spectrochim Acta A* 280:121538. <https://doi.org/10.1016/j.saa.2022.121538>
30. Ji YY, Zou X, Wang WJ, Wang TF, Zhang SL, Gong ZJ (2021) Co-doped S, N-Carbon dots and its fluorescent film sensors for rapid detection of Cr(VI) and ascorbic acid. *Microchem J* 167:106284. <https://doi.org/10.1016/j.microc.2021.106284>
31. Wang Q, Zhang SR, Zhong YG, Yang XF, Li Z, Li H (2017) Preparation of yellow-green-emissive carbon dots and their application in constructing a fluorescent turn-on nanoprobe for imaging of selenol in living cells. *Anal Chem* 89(3):1734–1741. <https://doi.org/10.1021/acs.analchem.6b03983>
32. Jia J, Lu WJ, Li L, Gao YF, Jiao Y, Han H, Dong C, Shuang SM (2020) Orange-emitting N-doped carbon dots as fluorescent and colorimetric dual-mode probes for nitrite detection and cellular imaging. *J Mater Chem B* 8(10):2123–2127. <https://doi.org/10.1039/C9TB02934F>
33. Lu S, Sui L, Liu J, Zhu SJ, Chen A, Jin MX, Yang B (2017) Near-infrared photoluminescent polymer-carbon nanodots with two-photon fluorescence. *Adv Mater* 29(15):1603443. <https://doi.org/10.1002/adma.201603443>
34. Espina-Casado J, Fontanil T, Fernández-González A, Cal S, Obaya AJ, Díaz-García ME, Badía-Laiño R (2021) Carbon dots as multifunctional platform for intracellular pH sensing and bioimaging. In vitro and in vivo studies. *Sens Actuators B* 346:130555. <https://doi.org/10.1016/j.snb.2021.130555>
35. Yang Y, Wang CF, Shu Q, Xu N, Qi SQ, Zhuo SJ, Zhu CQ, Du JY (2022) Facile one-step fabrication of Cu-doped carbon dots as a dual-selective biosensor for detection of pyrophosphate ions and measurement of pH. *Spectrochim Acta A* 268:120681. <https://doi.org/10.1016/j.saa.2021.120681>
36. Huo XM, Shen HL, Xu YJ, Shao J, Liu R, Zhang ZY (2022) Fluorescence properties of carbon dots synthesized by different solvents for pH detector. *Opt Mater* 123:111889. <https://doi.org/10.1016/j.optmat.2021.111889>
37. Bhati A, Anand SR, Gunture, Garg AK, Khare P, Sonkar SK (2018) Sunlight-induced photocatalytic degradation of pollutant dye by highly fluorescent red-emitting Mg-N-embedded carbon dots. *ACS Sustain Chem Eng* 6(7):9246–9256. <https://doi.org/10.1021/acssuschemeng.8b01559>

38. Liu JJ, Li DW, Zhang K, Yang MX, Sun HC, Yang B (2018) One-step hydrothermal synthesis of nitrogen-doped conjugated carbonized polymer dots with 31% efficient red emission for in vivo imaging. *Small* 14(15):1703919. <https://doi.org/10.1002/smll.201703919>
39. Zou GY, Chen S, Liu NZ, Yu YL (2021) A ratiometric fluorescent probe based on carbon dots assembly for intracellular lysosomal polarity imaging with wide range response. *Chin Chem Lett* 33(2):778–782. <https://doi.org/10.1016/j.ccllet.202108.076>
40. Ge JC, Jia QY, Liu WM, Guo L, Liu QY, Lan MH, Zhang HY, Meng XM, Wang PF (2015) Red-emissive carbon dots for fluorescent, photoacoustic, and thermal theranostics in living mice. *Adv Mater* 27(28):4169–4177. <https://doi.org/10.1002/adma.201500323>
41. Xu HB, Zhou SH, Xiao L, Wang HH, Li SZ, Yuan QH (2015) Fabrication of a nitrogen-doped graphene quantum dot from MOF-derived porous carbon and its application for highly selective fluorescence detection of Fe³⁺. *J Mater Chem* 3(2):291–297. <https://doi.org/10.1039/C4TC01991A>
42. Shi BF, Su YB, Zhang LL, Liu RJ, Huang MJ, Zhao SL (2016) Nitrogen-rich functional groups carbon nanoparticles based fluorescent pH sensor with broad-range responding for environmental and live cells applications. *Biosens Bioelectron* 82:233–239. <https://doi.org/10.1016/j.bios.2016.04.003>
43. Liu XX, Liu JR, Zheng BZ, Yan L, Dai JY, Zhuang ZJ, Du J, Guo Y, Xiao D (2017) N-doped carbon dots: green and efficient synthesis on a large-scale and their application in fluorescent pH sensing. *New J Chem* 41(19):10607–10612. <https://doi.org/10.1039/C7NJ01889D>
44. Wang K, Wang XY, Liu XY, Li ES, Zhao RS, Yang SH (2022) Facile synthesis of dual emission carbon dots for the ratiometric fluorescent detection of 2, 4, 6-trinitrophenol and cell imaging. *J Mol Struct* 1263(2022):133167. <https://doi.org/10.1016/j.molstruc.2022.133167>
45. Luo X, Yang HT, Wang HL, Ye ZW, Zhou ZN, Gu LY, Chen JQ, Xiao Y, Liang XW, Qian XH, Yang YJ (2018) Highly sensitive hill-type small-molecule pH probe that recognizes the reversed pH gradient of cancer cells. *Anal Chem* 90(9):5803–5809. <https://doi.org/10.1021/acs.analchem.8b00218>
46. Chen YC, Zhu CC, Cen JJ, Bai Y, He WJ, Guo ZJ (2015) Ratiometric detection of pH fluctuation in mitochondria with a new fluorescein/cyanine hybrid sensor. *Chem Sci* 6:3187–3194. <https://doi.org/10.1039/C4SC04021J>
47. Li B, Ma H, Zhang B, Qian J, Cao T, Feng HT, Li W, Dong YP, Qin WW (2019) Dually emitting carbon dots as fluorescent probes for ratiometric fluorescent sensing of pH values, mercury (II), chloride and cr (VI) via different mechanisms. *Microchim Acta* 186(6):1–10. <https://doi.org/10.1007/s00604-019-3437-2>
48. Lei XX, Fu YY, Wu Y, Chen L, Liang JG (2020) A ratiometric fluorescent probe for pH detection based on Ag₂S quantum dots-carbon dots nanohybrids. *Roy Soc Open Sci* 7(7):200482. <https://doi.org/10.1098/rsos.200482>
49. Wang XY, Wang YS, Pan W, Wang JP, Sun XB (2021) Carbon-dot-based probe designed to detect intracellular pH in fungal cells for building its relationship with intracellular polysaccharide. *ACS Sustain Chem Eng* 9(10):3718–3726. <https://doi.org/10.1021/acssuschemeng.0c08160>
50. Shanguan JF, He DG, He XX, Wang K, Xu FZ, Liu JQ, Tang JL, Yang X, Huang J (2016) Label-free carbon-dots-based ratiometric fluorescence pH nanoprobe for intracellular pH sensing. *Anal Chem* 88(15):7837–7843. <https://doi.org/10.1021/acs.analchem.6b01932>
51. Chen YY, Zhao CX, Wang YY, Rao HB, Lu ZW, Lu CF, Shan Z, Ren B, Wu W, Wang XX (2020) Green and high-yield synthesis of carbon dots for ratiometric fluorescent determination of pH and enzyme reactions. *Mat Sci Eng C* 117(1–2):111264. <https://doi.org/10.1016/j.msec.2020.111264>
52. Song JQ, Zhao N, Qu Y, Zhao LS (2021) Natural deep eutectic solvent-assisted preparation of nitrogen-doped carbon dots for ratiometric determination of pirimicarb and pH. *Dyes Pigm* 193:109564. <https://doi.org/10.1016/j.dyepig.2021.109564>
53. Li SR, Song XR, Hu ZR, Feng GD (2021) A carbon dots-based ratiometric fluorescence probe for monitoring intracellular pH and bioimaging. *J Photoch Photobio A* 409:113129. <https://doi.org/10.1016/j.jphotochem.2021.113129>

Publisher's Note Springer Nature remains neutral with regard to jurisdictional claims in published maps and institutional affiliations.

Springer Nature or its licensor (e.g. a society or other partner) holds exclusive rights to this article under a publishing agreement with the author(s) or other rightsholder(s); author self-archiving of the accepted manuscript version of this article is solely governed by the terms of such publishing agreement and applicable law.